remote sensing

MDPI

Article

Agreement Index for Burned Area Mapping: Integration of Multiple Spectral Indices Using Sentinel-2 Satellite Images

Daniela Smiraglia [1], Federico Filipponi [1,*], Stefania Mandrone [1], Antonella Tornato [1] and Andrea Taramelli [1,2]

[1] Institute for Environmental Protection and Research (ISPRA), via Vitaliano Brancati 48, 00144 Roma, Italy; daniela.smiraglia@isprambiente.it (D.S.); stefania.mandrone@isprambiente.it (S.M.); antonella.tornato@isprambiente.it (A.T.); andrea.taramelli@isprambiente.it (A.T.)

[2] Istituto Universitario di Studi Superiori di Pavia (IUSS), Palazzo del Broletto, Piazza della Vittoria 15, 27100 Pavia, Italy

* Correspondence: federico.filipponi@isprambiente.it; Tel.: +39-065-007-2438

Received: 29 April 2020; Accepted: 6 June 2020; Published: 8 June 2020

Abstract: Identifying fire-affected areas is of key importance to support post-fire management strategies and account for the environmental impact of fires. The availability of high spatial and temporal resolution optical satellite data enables the development of procedures for detailed and prompt post-fire mapping. This study proposes a novel approach for integrating multiple spectral indices to generate more accurate burned area maps by exploiting Sentinel-2 images. This approach aims to develop a procedure to combine multiple spectral indices using an adaptive thresholding method and proposes an agreement index to map the burned areas by optimizing omission and commission errors. The approach has been tested for the burned area classification of four study areas in Italy. The proposed agreement index combines multiple spectral indices to select the actual burned pixels, to balance the omission and commission errors, and to optimize the overall accuracy. The results showed the spectral indices singularly performed differently in the four study areas and that high levels of commission errors were achieved, especially for wildfires which occurred during the fall season (up to 0.93) Furthermore, the agreement index showed a good level of accuracy (minimum 0.65, maximum 0.96) for all the study areas, improving the performance compared to assessing the indices individually. This suggests the possibility of testing the methodology on a large set of wildfire cases in different environmental conditions to support the decision-making process. Exploiting the high resolution of optical satellite data, this work contributes to improving the production of detailed burned area maps, which could be integrated into operational services based on the use of Earth Observation products for burned area mapping to support the decision-making process.

Keywords: mapping post-fire; burned area; index threshold; spectral indices combination; Sentinel-2

1. Introduction

From the 1980s onwards, because of climate change conditions [1] and the increase in drought and land degradation phenomena [2], fires have become an important cause of land cover modifications around the world [3], affecting landscape patterns and functions [4–6], ecosystem processes [7,8], and air quality [9]. Identifying burnt areas provides key information on the extension of wildfires, the spatial location of the events, and the vegetation loss, which is useful to understand and quantify post-fire phenomena, such as air emissions, soil erosion, and vegetation recovery.

Earth Observation (EO) has proven to be a suitable technology for identifying areas affected by fire [10], from global [11,12] to local scales [13]. From this perspective, EO data have been used in the

identification of active fires [14–16], for delimiting the perimeters of burned areas [12,13,17], to monitor the recovery of vegetation after the event [18–21], and to determine the distribution of the plume in the atmosphere [22]. Furthermore, the identification of burned areas plays a key role in the estimation of atmospheric emissions during wildfires. Indeed, the global interannual variability in terrestrial ecosystem fluxes and in atmospheric CO_2 are strongly influenced by forest fire emissions [23,24].

The new generation of Copernicus satellite sensors for EO provides a high spatial, spectral, and temporal resolution; these satellites are useful to support the mapping of burned areas at detailed scales, such as the Multispectral Instrument (MSI) sensor aboard Sentinel-2 (S2) satellites, which is also equipped with spectral bands in the red-edge domain. The red-edge bands are of great importance for improving vegetation characterization [25,26] and for the development of new spectral indices for the detection of burned areas [27], which are areas that show changes in forest and grassland biomass that can be detected by EO instruments [28]. Such distinguishing features of S2 satellites enable the development of procedures for detailed and prompt operational services based on post-fire mapping, as promoted, for example, by the European Union in the framework of the Copernicus Emergency Management Service (Copernicus EMS Wildfire rapid mapping: https://emergency.copernicus.eu/mapping; European Forest Fire Information System (EFFIS): https://effis.jrc.ec.europa.eu). The image analysis methods used for the recognition of burned areas focus on the effects of vegetation modifications due to fire [15,29,30]. A multitemporal analysis to detect changes in vegetation has proved to be more effective than single-image analysis [17,31,32].

Spectral indices (SIs) obtained by the combination of bands are used to differentiate between the post- and pre-fire images, discriminating between burned and unburned areas. Notwithstanding the fact that they have been widely used for burned area mapping [31], it is difficult to identify the most suitable index. In addition, research studies generally evaluate the performances of SIs on ideal case studies—i.e., wildfires occurring during the summer dry season when the vegetation is still photosynthetically active—without demonstrating whether they perform well under different environmental conditions. In fact, one SI may be more suitable than others only under specific conditions, because the spectral response depends on many factors (e.g., atmospheric conditions, satellite image characteristics, and the date of image acquisition after the fire event) including the site conditions (e.g., pre-fire soil and vegetation types, vegetation phenological stage, season); besides this, the index threshold choice is often not objective and flexible enough to be adapted to the local conditions [13,33–36]. Even though many SIs have good spectral separability in detecting wildfires that occur during the summer dry season, when the vegetation is still photosynthetically active, and for identifying spatially comparable burned areas, their detection performances could be quite different for other seasons or under different environmental conditions.

The integration of multiple SIs could provide a solution to take advantage of different spectral band combinations and optimize the detection of burned areas. The assessment, comparison, and integration of multiple SIs have been widely applied to reduce commission errors [37,38], although the results are still affected by the site-specific environmental characteristics [39]. Each biome is determined by specific abiotic and biotic environmental factors [6,40,41] and is characterized by different vegetation types with different structural, phenological, and physiological traits [42,43]. Consequently, measured parameters, such as SI performance, can vary greatly across biomes [43] and seasons. While there is a large body of literature about the comparison of multiple SIs' performances [33,44–47], only a few studies have attempted to integrate different SIs for burned area mapping, using methodological approaches, such as decision rules, based on the optimization of omission and commission errors [31], on adaptive thresholding combined with decision rules [12], the intersection method [48], the iterative self-organizing data analysis technique algorithm [49], and on soft integration using fuzzy scores [13,50,51].

This research study introduces an approach based on the spatially explicit Agreement IndeX (AIX), which can be consistently used to integrate multiple SIs for burned area mapping. Most of the operational services based on the use of EO products for burned area mapping (i.e., EFFIS) make use

of medium-resolution optical satellite data analyzed with methodological approaches that make use of predefined sets of parameters and a constant number of SIs. The production of detailed burned area maps exploiting high-resolution optical satellite data, such as S2, and taking advantage of parameter tuning is yet to be accomplished. The operational service procedures could integrate the AIX approach to increase detailed wildfire mapping capacity for sites with different environmental conditions in all the fire seasons, balancing the errors, and optimizing the accuracy. This study aims to propose a procedure for burned area mapping through the combination of multiple SIs that i) identifies the best SI to be used to define SI thresholding based on the fire season and site conditions; ii) use an adaptive SI thresholding method which is flexible enough to be adapted to the local conditions, and iii) introduce a spatially explicit agreement index that can be consistently used for areas with different environmental conditions in all fire seasons.

After introducing the topic of burned area mapping through EO data and the use of SI, we demonstrate the effectiveness of the procedure in four case studies, consisting of distinct wildfires that occurred during different seasons in areas with different environmental characteristics. We describe the input data used and the method applied for analyzing S2 images and for computing the proposed index. The results section shows the SIs' performances and the final burned area map, and then we discuss the results of the analysis taking into account the advantages and shortcomings of the procedure. Finally, we summarize the derived conclusions.

2. Materials and Methods

2.1. Study Area

The procedure was developed at a local scale in Italy, and four burned areas were chosen from the archive of fire events made available by the Carabinieri Forestali (CUFAA, https://www.carabinieri.it/arma/oggi/organizzazione/organizzazione-per-la-tutela-forestale-ambientale-e-agroalimentare): One fire was located in the municipality of Bussoleno, and one was in the municipality of Trivero, both of which were in the Piedmont region in northern Italy; one was in the municipality of Roccagorga in central Italy, and the last was in the municipality of Gravina in Puglia, located in southern Italy (Figure 1). The CUFAA wildfire database responds to Italian law (http://www.parlamento.it/parlam/leggi/00353l.htm) and reports information about the burned area surface extent and the burned vegetation. To test the methodology across various contexts, we selected study areas that differ in environmental conditions (climate, lithology, geomorphology, vegetation), land use, and fire season. In this study, the polygon representation of the four burned areas obtained from the fire events' archive was used in the procedure. The four polygons represented in Figure 1 are the reference maps used to detect the best SI, to identify the SI threshold, to compute the AIX score, and to validate the results.

Bussoleno and Trivero are situated in the Alpine mountain range. The fire events occurred in 2017 and 2015, respectively, both during the fall season and after an extended drought season. Roccagorga and Gravina in Puglia are situated in the Apennine mountain range, and the fire events occurred during a harsh summer dry season in 2017. The characteristics of the study areas and the information about the fire events are reported in Table 1.

2.2. Satellite Images

EO data used for the identification of burned areas in the study areas were acquired by Sentinel-2A and Sentinel-2B satellites. The Copernicus Sentinel-2 (S2) is a satellite mission carrying the Multi-Spectral Instrument (MSI) multispectral sensor with a high spatial resolution (10 m, 20 m and 60 m), high revisit capability (5 days with two satellites), an orbital swath width of 290 km and a moderately large band set (13 spectral bands) from the visible to shortwave infrared (https://sentinel.esa.int/web/sentinel/missions/sentinel-2/instrument-payload/resolution-and-swath) (Table S1).

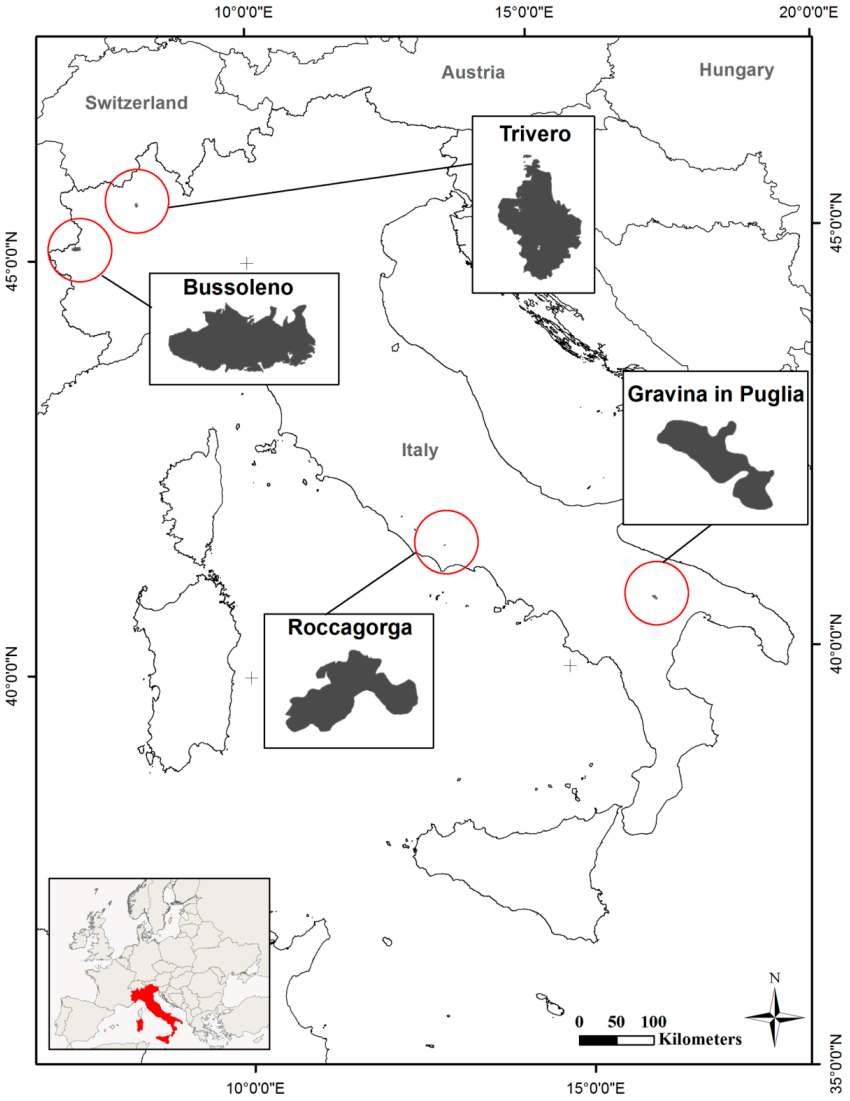

Figure 1. Location of the study areas.

Table 1. Environmental characteristics and fire event information of the four study areas.

Study Area	Climate [52] and Lithomorphology [53]	Vegetation (CUFAA)	Start Date–End Date (CUFAA)	Fire Extension (CUFAA)	Elevation Range a.s.l. (CUFAA)
Bussoleno	- Temperate semi-continental–oceanic - Metamorphic slopes	- Coniferous forest (evergreen and deciduous) - Oak and beech forest - Grasslands	2017-10-22–2017-11-02	4000 ha	600–2700
Trivero	- Temperate oceanic - Igneous intrusive slopes	- Beech forest - Shrublands	2015-11-27–2015-12-06	1000 ha	700–1800
Roccagorga	- Transitional Mediterranean oceanic - Carbonate slopes	- Pine forest - Shrublands - Grasslands	2017-07-21–2017-07-22	80 ha	450–900
Gravina in Puglia	- Mediterranean oceanic–semi-continental - Sedimentary clastic table-land	- Pine forest - Oak forest - Shrublands - Grasslands	2017-08-12–2017-08-14	1300 ha	350–450

Pre-fire and post-fire S2 L2A products were downloaded from the Theia catalog (https://theia.cnes.fr/atdistrib/rocket/#/home) for each study area (Table 2). False-color maps generated from selected pre-fire and post-fire images are shown in Figure 2. The spectral bands available and the spatial resolution of 10 m for the visible–near-infrared range (VIS-NIR) and 20 m for red-edge–shortwave infrared range (red-edge-SWIR) enable detailed detection when applying SIs which are usually used for identifying burned areas (Table S1).

Table 2. Pre- and post-fire tiles and acquisition date and time for the four study areas.

Study Area	Tile Name	Acquisition Date	Acquisition Time	Satellite
Bussoleno	T32TLR	2017-10-17	10:30:24	S2A
	T32TLR	2017-11-21	10:33:23	S2B
Trivero	T32TMR	2015-11-24	10:23:39	S2A
	T32TMR	2015-12-17	10:39:53	S2A
Roccagorga	T33TUG	2017-07-20	10:00:27	S2A
	T33TUG	2017-07-30	10:05:35	S2A
Gravina in Puglia	T33TXF	2017-08-11	09:55:12	S2B
	T33TXF	2017-08-18	09:40:28	S2B

2.3. Methods

All the spectral bands of the images, distributed in the MUSCATE format as the bottom of the atmosphere (BOA) reflectances, which were orthorectified, terrain-flattened, and atmospherically corrected with MACCS-ATCOR Joint Algorithm (MAJA) [54,55], were processed for spatial resampling at 20 m and for the masking of topographic shadows. The images correspond to the bottom of the atmosphere reflectances, which were corrected for topographic effects to avoid the spectral variability originating from the local topography. The areas corresponding to topographic shadows (identified by product quality flags representing the topographic mask and low-sun mask, with the latter considering the pixel aspect, slope, and sun zenith angle) were not considered in the analysis and, therefore, also excluded from the reference maps. In this study, only the Trivero and Bussoleno areas showed topographic shadows and needed masking.

Resampled and masked images were used to compute SI before and after the fire event. Five SIs were used to recognize burned areas, which were chosen to cover the VIS/red-edge/NIR/SWIR spectral ranges (Table 3):

Table 3. Spectral indices adopted, equations with Sentinel-2 Multispectral Instrument (MSI) bands, and bibliographic references.

Spectral Index	Equation	Reference
NBR Normalized Burn Ratio	$\frac{B12-B8}{B12+B8}$	[30,56,57]
NBR2 Normalized Burn Ratio 2	$\frac{B12-B11}{B12+B11}$	[20,58]
MIRBI Mid-Infrared Bispectral Index	$10 * B12 - 9.8 * B11 + 2$	[59]
BAIS2 Burned Area Index for Sentinel-2	$1 - \left(\sqrt{\frac{B6*B7*B8A}{B4}}\right) * \left(\frac{B12-B8A}{\sqrt{B12+B8A}} + 1\right)$	[17,27]
NDVI Normalized Difference Vegetation Index	$-\left(\frac{B8A-B4}{B8A+B4}\right)$	[60]

The original formulae for the Normalized Burn Ratio (NBR) and Normalized Difference Vegetation Index (NDVI) have been modified to make the behavior of the indices consistent: The values of all the indices increased if the pixel was affected by fire. The NDVI formula uses B8A instead of B8 since it provides more precise spectral information.

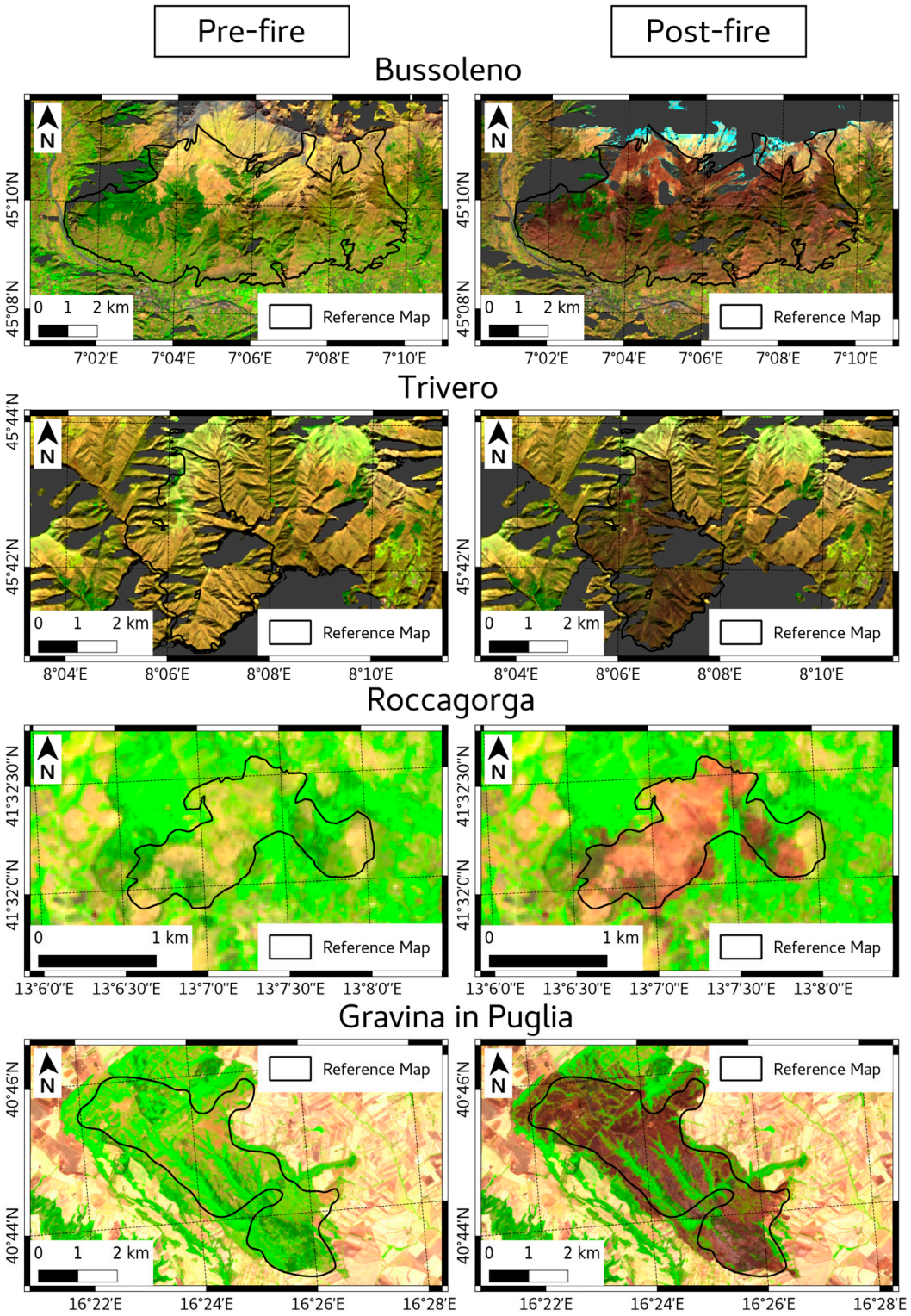

Figure 2. Maps of pre-fire and post-fire S2 images displayed in false color (R: bottom of the atmosphere (BOA) reflectance at 1610 nm; G: BOA reflectance at 864 nm; B: BOA reflectance at 665 nm). The solid line represents the polygon contour of the burned area reference map. The grey color represents areas affected by topographic shadows. The dates of the images are the acquisition dates shown in Table 2.

Image differencing was performed [61] through the arithmetic difference between post-fire and pre-fire index values ($\Delta_{\text{post-pre}}$ images) to detect abrupt changes and retrieve burned pixels. Regarding the difference SIs (i.e., dNBR, dNBR2, Mid-Infrared Bispectral Index (dMIRBI), Burned Area Index for

Sentinel-2 (dBAIS2), and dNDVI), a set of thresholds was applied to obtain a first set of burned/not burned maps.

Index thresholds were defined, starting from a spectral sensitivity analysis to assess the efficacy of SI to separate burned and unburned land. The separability index (M) was applied as follows (Equation (1)) [33,62,63]:

$$M = \frac{\mu b - \mu u}{(\sigma b + \sigma u)} \quad (1)$$

where μb and μu are the mean values of the difference SIs for burned and unburned pixels, and σb and σu are the standard deviations of the difference SIs. M values higher than 1 indicate a good separability between burned and unburned land [62]. To calculate the M index, the analysis was performed on an area of around 10 times the surface of the burned polygon defined in the reference map.

The threshold values were identified, starting from the polygons obtained from the difference SI with the highest M value. The median SI values of the pixels on the polygon contour and adjacent to polygon contour (inside and outside) of the reference map were calculated (Figure 3). The empirical threshold value of the difference SI with the highest M value chosen by an expert is a value derived by the statistic distribution of the pixels inside, outside, and on the contour of the reference map.

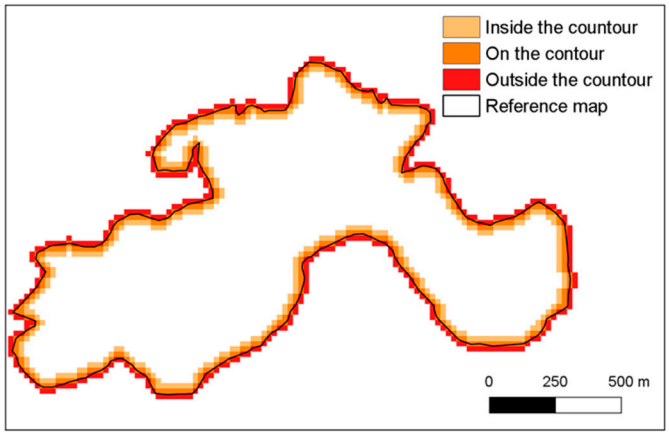

Figure 3. Example of pixel distribution inside, outside, and on the contour of the reference map.

Threshold values for the other SIs were calculated through an adaptive procedure by applying the regression equation of each difference SI vs. the difference SI with the highest M value, considered as the best SI. After that, the binary images classified as burned (pixels above the threshold value) and unburned (pixels below the threshold value) could be defined. The accuracy assessment for each difference SI was calculated using confusion matrices comparing the resulting maps against the reference maps. Omission and commission error estimation was performed.

To define the final burned area map, an Agreement IndeX (AIX) was proposed by combining the SIs as described in Equation (2):

$$AIX = \frac{\sum_{i=1}^{N} P_{SI}}{N} \quad (2)$$

where P is a burned pixel, SI is the spectral index, and N is the number of SIs. The optimum combination of SIs to use to obtain the final map is the one that optimizes the error of each difference SI (both omission and commission) and the overall classification accuracy.

For each combination of n SIs corresponding to a different AIX value, the overall accuracy and omission, commission, and total errors were calculated from a comparison with the reference map. In addition, an Agreement Index Score (AIS) was computed according to Equation (3):

$$AIS = ((1 - OE) + (1 - CE)) * OA \quad (3)$$

where *OE* is the omission error, *CE* is the commission error, and *OA* is the overall classification accuracy. The AIS serves to identify the AIX value, which corresponds to a combination of *n* SIs that balances the errors and optimizes the accuracy. The final burned area map is the result of the pixels for which the combination of at least *n* SIs out of *N* identifies them as burned pixels.

Figure 4 shows the workflow of the main phases of the procedure: (1) pre-processing and (2) the identification of burned areas. All the analyses were performed using R-CRAN and Quantum GIS 3.4 software.

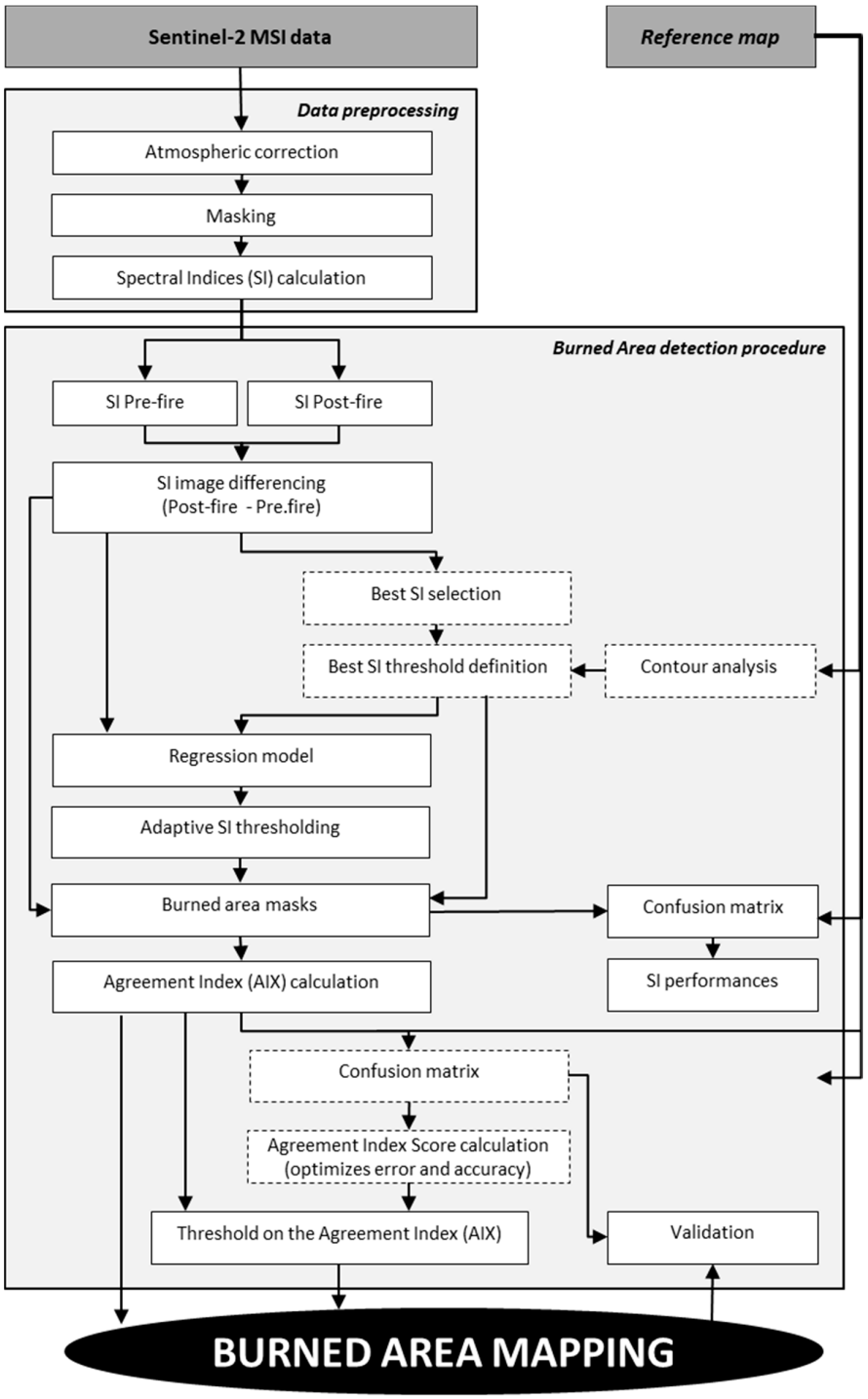

Figure 4. Workflow of the main phases of the procedure for burned area mapping. Dashed line boxes refer to training phases. SI: spectral index.

3. Results

Regarding the separability index (*M*), dNBR2 was the index that showed the highest discriminant power for the two study areas of Bussoleno and Gravina in Puglia and dNBR was the index that showed the highest discriminant power for the Roccagorga study area, whereas the dMIRBI index showed the highest *M* value for the Trivero study area. The resulting separability index (*M*) values for all the study areas are reported in Table 4; the highest values for each study area are shown in bold.

Table 4. Separability indices (*M*) of the spectral indices.

Spectral Index	Bussoleno	Trivero	Roccagorga	Gravina in Puglia
dNBR	0.58845	0.85566	**1.28991**	1.24775
dNBR2	**0.85765**	1.21820	1.27707	**1.31510**
dMIRBI	0.76930	**1.26844**	0.99870	1.14082
dBAIS2	0.57760	0.96142	1.28847	1.25714
dNDVI	0.29361	0.11608	1.19782	1.03085

Having obtained the highest *M* value, dNBR and dNBR2 were selected as the best SIs to serve as reference for the summer dry season study cases (Roccagorga and Gravina in Puglia), while dMIRBI and dNBR2 were selected as reference SIs for the fall dry season (Trivero and Bussoleno). These SIs were used to identify the empirical threshold for the study areas, and the median values of the pixels on the boundary and adjacent to the boundary (inside and outside) of the reference maps were calculated (Table 5).

Table 5. Median (Med) and median absolute deviation (MAD) values of the pixels outside the boundary, on the boundary, and inside the boundary of the reference maps of the study areas, and the thresholds chosen by expert-based evaluation.

Study Area	Spectral Index	Outside the Boundary		On the Boundary		Inside the Boundary		Threshold
		Med	MAD	Med	MAD	Med	MAD	
Bussoleno	dNBR2	0.064	0.0323	0.076	0.0345	0.091	0.0364	0.08
Trivero	dMIRBI	0.085	0.1078	0.165	0.1368	0.329	0.1737	0.20
Roccagorga	dNBR	0.148	0.1174	0.226	0.1430	0.291	0.1254	0.15
Gravina in Puglia	dNBR2	0.157	0.0832	0.171	0.0806	0.182	0.0822	0.18

SI thresholds, estimated using regression equations in the adaptive thresholding processing step, were computed starting from the thresholds defined for the best SI and reported in Table 5.

Table 6 reports the SIs' performances by providing the estimated threshold values of all the difference SIs and the omission and commission errors and overall accuracies for each burned area map, with the highest values shown in bold. Figures S1–S4 show the $\Delta_{\text{post-pre}}$ and the classified burned/not burned images of each difference SI for the four study areas. Regarding the Bussoleno burned area maps, the highest overall accuracies of 0.57 were achieved by dBNR2 and dMIRBI, whereas for the Trivero study case, dMIRBI and dNBR2 achieved the highest overall accuracies (0.65 and 0.61, respectively). Both areas showed a high commission error for all the indices, especially Trivero. Regarding the Roccagorga burned areas maps, an overall accuracy of 0.96 was achieved by dNBR and dNDVI, while the dMIRBI results showed an overestimation of the burned surfaces, and dNBR2 showed the lowest omission error. The study case of Gravina in Puglia showed high overall accuracy for all the indices (dNBR, dNBR2, and dBAIS2 achieved 0.93) as well as the lowest commission errors; in particular, dNDVI achieved 0.17.

Table 7 reports the classification performances combining a different number of SIs. For all the study areas, the increment of the AIX value corresponded to an increase in the omission error and a reduction in the commission error. In contrast, a higher overall accuracy value can result from the combination of different SIs. The AIS has the capability to combine both the total error (omission error

and commission error) and the overall accuracy. Three study areas out of four resulted in a higher AIS with the combination of four SIs. The Gravina di Puglia study area reported a higher AIS (1.43) when only one SI was considered. The resulting number of SI combinations balanced the omission, commission, and total errors.

Table 6. Index thresholds, omission and commission errors, and overall accuracies for the produced burned areas maps.

Study Area	Spectral Index	Index Threshold	Omission Error	Commission Error	Overall Accuracy
Bussoleno	dNBR	0.17811	0.25617	0.59035	0.50137
	dNBR2	0.08000	0.20319	0.42630	**0.57173**
	dMIRBI	0.24750	0.22810	0.42883	**0.57004**
	dBAIS2	0.10419	0.25069	0.60330	0.49316
	dNDVI	0.15673	0.43883	0.69454	0.45251
Trivero	dNBR	0.02911	0.16533	0.82592	0.54387
	dNBR2	0.01287	0.08047	0.67916	**0.61069**
	dMIRBI	0.20000	0.15396	0.46814	**0.64666**
	dBAIS2	0.02644	0.15438	0.77732	0.57587
	dNDVI	0.07412	0.46000	0.93336	0.42093
Roccagorga	dNBR	0.15000	0.16636	0.20783	**0.96287**
	dNBR2	0.05340	0.15768	0.24661	0.95821
	dMIRBI	0.17666	0.26177	0.44008	0.91882
	dBAIS2	0.09405	0.16326	0.21936	**0.96159**
	dNDVI	0.08408	0.17472	0.22355	**0.96024**
Gravina in Puglia	dNBR	0.36187	0.29721	0.19421	**0.93050**
	dNBR2	0.18000	0.29446	0.18933	**0.93160**
	dMIRBI	0.53050	0.35442	0.21729	0.92053
	dBAIS2	0.21710	0.28462	0.20447	**0.93022**
	dNDVI	0.20464	0.36463	0.17008	0.92630

Note: Figures S1–S4 show the $\Delta_{\text{post-pre}}$ and the classified burned/not burned images of each different SI for the four study areas.

Table 7. Number of Spectral Index (SI) combinations, Agreement IndeX (AIX) classes, omission and commission errors, overall accuracy, total error, and Agreement Index Score (AIS) of the study cases. The selected SI combination used to generate the final burned area map is shown in bold.

Study Area	SI	AIX	Omission Error	Commission Error	Overall Accuracy	Total Error	AIS
Bussoleno	1	>=0.2	0.15682	0.67286	0.53281	0.82968	0.62355
	2	>=0.4	0.22073	0.60890	0.59720	0.82963	0.69895
	3	>=0.6	0.28272	0.53317	0.64398	0.81589	0.76254
	4	**>=0.8**	**0.34470**	**0.40699**	**0.68729**	**0.75170**	**0.85795**
	5	=1	0.61131	0.23673	0.69611	0.84804	0.80189
Trivero	1	>=0.2	0.04100	0.91096	0.36407	0.95196	0.38156
	2	>=0.4	0.08080	0.81790	0.54567	0.89870	0.60094
	3	>=0.6	0.14426	0.71530	0.60730	0.85956	0.69259
	4	**>=0.8**	**0.21627**	**0.48889**	**0.65005**	**0.70516**	**0.84171**
	5	=1	0.57412	0.20937	0.65903	0.78349	0.80172
Roccagorga	1	>=0.2	0.14157	0.45453	0.91738	0.59610	1.28791
	2	>=0.4	0.15520	0.24313	0.95887	0.39834	1.53579
	3	>=0.6	0.16636	0.21408	0.96207	0.38043	1.55813
	4	**>=0.8**	**0.17813**	**0.19630**	**0.96347**	**0.37443**	**1.56619**
	5	=1	0.28253	0.15628	0.95995	0.43881	1.49866
Gravina in Puglia	**1**	**>=0.2**	**0.24300**	**0.22162**	**0.93180**	**0.46462**	**1.43066**
	2	>=0.4	0.27420	0.20573	0.93125	0.47993	1.41556
	3	>=0.6	0.29569	0.19413	0.93078	0.48981	1.40566
	4	>=0.8	0.32716	0.18282	0.92895	0.50998	1.38414
	5	=1	0.45529	0.15999	0.91685	0.61528	1.26957

Figure 5 shows the spatial distribution of the AIX classes and the final maps of burned areas; that is, the pixels which the combination of *n* SIs identified as belonging to the "burned" class.

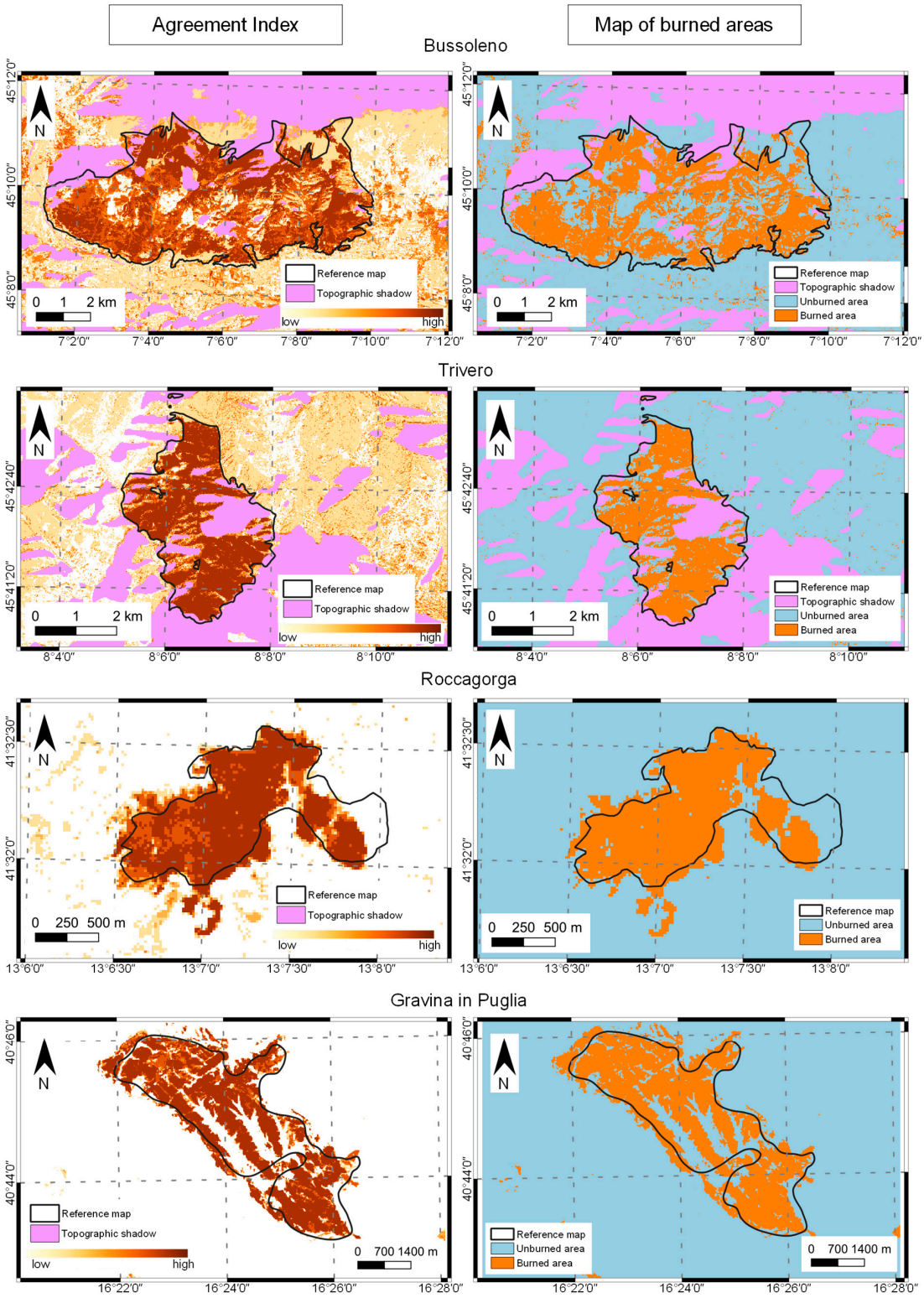

Figure 5. Spatial distribution of the Agreement IndeX (AIX) and maps of burned areas for the four study cases.

4. Discussion

In this research, we compared various case studies in four areas with diverse site conditions to evaluate the performances of different SIs for the burned area mapping of wildfires, which occurred in different seasons and under different environmental conditions in terms of climate, geomorphology, and vegetation cover. In fact, two wildfires occurred during the winter season in areas with vegetation cover characterized by grasslands and deciduous forest. Other considered wildfires occurred during the summer dry season: The Roccagorga study case mostly involved a natural area also covered by shrublands and grasslands, while Gravina in Puglia could be considered an ideal study case, where the wildfire burned a natural forest with both deciduous and evergreen tree species. The wildfires which occurred during the fall and winter seasons in the Alps also highlighted the need for a proper topographic shadows mask [17], with the capacity to remove dark pixels from further processing and reduce the commission error in the classification phase.

Research studies generally evaluate the performances of SIs on ideal case studies [44–46]—i.e., wildfires occurring during the summer dry season, when the vegetation is still photosynthetically active—but the results could differ from other case studies, especially for SIs that rely on vegetation greenness (e.g., NDVI), and that could not perform well if a fire event occurs at the end of the senescence phase. Our results demonstrate that SIs have different performances under different environmental conditions. In some circumstances, the same SI performs best in one study area and worst in another study case. Vegetation SIs, such as dNDVI and dBAIS2, have a reduced detection capability in deciduous tree species during the fall and winter dry seasons due to the poor photosynthetic activity. Indeed, dNDVI showed a high omission error, and both indices had large commission errors for Bussoleno and Trivero study cases since the burned area was mainly represented by deciduous forests at the end of the senescence phase. dBAIS2 generally has a discrete detection capability for grasslands, while it has a good detection capability for Mediterranean mixed vegetation (e.g., the study case of Gravina in Puglia). dNBR was revealed to be a good SI; in particular, it obtained the best performances for herbaceous environments. dMIRBI exhibited good performance during the fall dry season, whereas dNBR2 showed generally good performance in all the cases and was shown to be suitable for fall and winter seasons.

The integration of SIs was performed on a pixel base with the numerical support of the AIX. This is a spatially explicit methodology that could be adapted to different site conditions as appropriate. The two considered summer study cases reported a high overall accuracy, exceeding the value of 0.9 for all SI combinations. The results obtained for the Gravina in Puglia area—here considered an ideal study case—showed high AIS, high overall accuracy values, and low commission error values, even using a single SI. Since the commission error generated by each SI was very low, burned area identification for summer wildfires could benefit less from SI integration than a fire that occurs in other seasons. On the contrary, fall season study cases showed the need for an in-depth investigation to avoid a different phenology leading to erroneous evaluations. The support of the AIX allowed us to obtain higher overall accuracies and, at the same time, to lower the omission errors compared to considering the SIs separately. Another research study [33] attempted to integrate multiple SIs: After performing an SI separability analysis, SI values were reduced to a common domain, converted to positive and negative evidence [38], and integrated using fuzzy membership functions; finally, burned area pixels were identified, applying different operators, such as ordered weighted averaging [51]. Alternatively, research studies using multiple SIs adopted a set of empirical conditional statements, also defined as decision rules, to identify burned area maps [31] even with the support of a temporal harmonizer algorithm [64], or use distribution-modeling algorithms trained by hyperspectral indexes and hotspots to model and map burned areas [47]. Compared to other methodologies described in the literature, the approach presented in this study has the strengths of significantly reducing the use of pre-defined set of parameters, thanks to the adaptive thresholding, and rejecting the use of SIs whose mapping performances are not adequate for specific site conditions, thanks to the AIX.

The proposed procedure first identifies the most suitable SI to be used as a reference, then calculates thresholds for the other SIs based on regression models, and computes a single burned area mask from each SI. Later, all the burned area masks are combined to calculate the AIX, which is finally used to map the burned areas by optimizing omission and commission errors. The availability of reference maps supports the analysis by providing information for the identification of the best SI to be used for the index separability analysis, allowing us to determine the best SI threshold and calculate the AIS and classification accuracy metrics to support the selection of the number of SIs to be used for the final burned area map generation and for validation purposes. The procedure could be used in a training phase to evaluate the performances of SIs on a large set of wildfire cases for which a reference map is available. One may think that the pre-fire and post-fire images could be selected during the vegetation growing season, without the burn date; this could reduce, on the one hand, the commission error due to the slight variation in pre-fire and post-fire spectral signatures, but, on the other hand, this would consistently increase the omission error due to the vegetation restoration process [21]. It is, therefore, necessary to select the best-performing SIs, which may depend on the vegetative status, and to integrate all of them to obtain the most accurate mapping, balancing the omission and commission errors, and optimizing the overall accuracy. Compared to the methodologies available in the literature, the proposed approach allowed us to use a variable number of SIs, and it benefited from the best-performing SIs for the site-specific conditions, with the AIX selecting the number of SIs on a single pixel base.

In the procedure training phase, a reference map can be used to calculate the separability index and identify the SI that results in the most accurate burned area mapping and its threshold value. The identification of the best SI for specific site conditions allowed us to use it as the reference SI when using adaptive SI thresholding. Once the training phase is completed, the site conditions related to the time of the season and the phenology may be used to establish which SI and threshold value should be used, opening the way to a newer paradigm for the development of burned area mapping operational services. Here, the extensively adopted methodology for burned area mapping operational services was based on a defined set of SIs and the threshold to be used, independent of the site conditions [11,12]. Alternatively, operational services may use an automatic thresholding algorithm developed to exploit the statistical bimodal distribution analysis [49]. Further analysis is still required to create a dictionary that suggests the SI and thresholds to be used under the different site conditions, fire regimes, and ecosystems, to move the proposed approach from training mode to operational mode. The availability of high-resolution land cover maps as ancillary information to identify vegetation cover type prior to a wildfire taking place could help to identify the parameters from the dictionary (SI, threshold, and AIX) to be used for the burned area mapping. Alternatively, on-demand high-resolution land cover mapping operational services can be adopted. The information regarding the land cover (especially dominant tree species) and vegetation status in the pre-fire stage can also integrate the burned area maps with indispensable information for the estimation of atmospheric emissions during wildfires [65].

5. Conclusions

In recent years, the high spatial and temporal resolution of EO data, such as the S2 satellite, has enabled progress in the development of detailed and timely post-fire mapping. The availability of detailed and prompt mapping of post-fire areas is important to support post-hazard management strategies, including soil erosion estimation, air emission control, and environmental loss recovery.

SIs are widely used for burned area mapping, although the choice of the best SIs, the threshold values and their performances are often assessed without taking into account the fire season, the local geomorphology, the vegetation types and their phenological stage.

This study proposed an approach for improving the detection of burned land using satellite optical multispectral data, taking advantage of different spectral bands through the combination of multiple SIs. The results are encouraging considering the high level of accuracy of the final maps achieved,

reducing the problems associated with under and overestimation. Moreover, the transferability of the procedure in different geographical contexts was verified by testing on different study cases, with satisfactory results, which highlight the potential for this method to be applied over larger areas.

The adaptive SI thresholding method and the proposed AIX could be applied to different site conditions and could represent a tool to link SIs, thresholds, and environmental conditions. The possibility to test the methodology on a large set of wildfire cases could allow a catalog to be created that encompasses the aspects mentioned above which are representative of the existing case studies and that could support operational services based on the use of EO products for burned area mapping in order to support the decision-making process.

Supplementary Materials: The following are available online at http://www.mdpi.com/2072-4292/12/11/1862/s1, Table S1: Spectral characteristics of the Sentinel-2 MSI sensor, Figure S1: Δpost-pre images and burned/not burned images of each difference SI for the Bussoleno study area, Figure S2: Δpost-pre images and burned/not burned images of each difference SI for the Trivero study area, Figure S3: Δpost-pre images and burned/not burned images of each difference SI for the Roccagorga study area, Figure S4: Δpost-pre images and burned/not burned images of each difference SI for the Gravina in Puglia study area.

Author Contributions: Conceptualization, D.S., F.F., S.M., and A.T. (Antonella Tornato); Methodology, D.S., F.F., and S.M.; Supervision, A.T. (Antonella Tornato) and A.T. (Andrea Taramelli); Visualization, D.S. and F.F.; Writing—original draft, D.S. and F.F.; Writing—review and editing, D.S., F.F., S.M., A.T. (Antonella Tornato), and A.T. (Andrea Taramelli). All authors have read and agreed to the published version of the manuscript.

Funding: The research was funded by the Italian Space Agency (ASI) in the framework of agreement between ASI and the Italian Institute for Environmental Protection and Research (ISPRA) on "Air Quality" (Agreement number F82F17000000005).

Acknowledgments: This work contains modified Copernicus Sentinel data and Copernicus Service information (2020). Sentinel 2 MSI data used were available at no cost from ESA Sentinels Scientific Data Hub. Copernicus Sentinel-2 data were processed at level 2A by CNES for THEIA Land data center. Successive data processing was performed through the LaViSAm (Laboratorio Virtuale dei Servizi Ambientali). The authors are grateful to the many individuals working on the development of free and open-source software for supporting the sharing of knowledge. They also wish to acknowledge the very useful and constructive comments by ISPRA colleagues Gianluca Leone, Marina Vitullo, and Giorgio Cattani.

Conflicts of Interest: The authors declare no conflict of interest.

References

1. Westerling, A.L.; Hidalgo, H.G.; Cayan, D.R.; Swetnam, T.W. Warming and earlier spring increase Western U.S. forest wildfire activity. *Science* **2006**, *313*, 940–943. [CrossRef] [PubMed]
2. Bajocco, S.; Salvati, L.; Ricotta, C. Land degradation versus fire: A spiral process? *Prog. Phys. Geogr.* **2011**, *35*, 3–18. [CrossRef]
3. Thonicke, K.; Venevsky, S.; Sitch, S.; Cramer, W. The role of fire disturbance for global vegetation dynamics: Coupling fire into a Dynamic Global Vegetation Model. *Glob. Ecol. Biogeogr.* **2001**, *10*, 661–677. [CrossRef]
4. Lloret, F.; Calvo, E.; Pons, X.; Díaz-Delgado, R. Wildfires and landscape patterns in the eastern Iberian peninsula. *Landsc. Ecol.* **2002**, *17*, 745–759. [CrossRef]
5. Viedma, O.; Moreno, J.M.; Rieiro, I. Interactions between land use/land cover change, forest fires and landscape structure in sierra de Gredos (Central Spain). *Environ. Conserv.* **2006**, *33*, 212–222. [CrossRef]
6. Turner, M.G.; Gardner, R.H. *Landscape Ecology in Theory and Practice. Pattern and Process*; Springer: New York, NY, USA, 2015; p. 482. [CrossRef]
7. Calvo, L.; Tárrega, R.; Luis, E. Secondary succession after perturbations in a shrubland community. *Acta Oecologica* **2002**, *23*, 393–404. [CrossRef]
8. Anderson, R.C. Evolution and origin of the Central Grassland of North America: Climate, fire, and mammalian grazers. *J. Torrey Bot. Soc.* **2006**, *133*, 626–647. [CrossRef]
9. French, N.H.F.; Kasischke, E.S.; Williams, D.G. Variability in the emissions of carbon-based trace gases from wildfire in the Alaskan boreal forest. *J. Geophys. Res.* **2003**, *107*, 8151. [CrossRef]
10. Chuvieco, E. *Earth Observation of Wildland Fires in Mediterranean Ecosystems*; Springer: Berlin/Heidelberg, Germany, 2009; p. 257. [CrossRef]

11. Bastarrika, A.; Alvarado, M.; Artano, K.; Martinez, M.P.; Mesanza, A.; Torre, L.; Ramo, R.; Chuvieco, E. BAMS: A Tool for Supervised Burned Area Mapping Using Landsat Data. *Remote Sens.* **2014**, *6*, 12360–12380. [CrossRef]
12. Roteta, E.; Bastarrika, A.; Padilla, M.; Storm, T.; Chuvieco, E. Development of a Sentinel-2 burned area algorithm: Generation of a small fire database for sub-Saharan Africa. *Remote Sens. Environ.* **2019**, *222*, 1–17. [CrossRef]
13. Boschetti, M.; Stroppiana, D.; Brivio, P.A. Mapping burned areas in a Mediterranean environment using soft integration of spectral indices from high-resolution satellite images. *Earth Interact.* **2010**, *14*, 1–20. [CrossRef]
14. Wooster, M.J.; Zhukov, B.; Oertel, D. Fire radiative energy for quantitative study of biomass burning: Derivation from the BIRD experimental satellite and comparison to MODIS fire products. *Remote Sens. Environ.* **2003**, *86*, 83–107. [CrossRef]
15. Schroeder, W.; Prins, E.; Giglio, L.; Csiszar, I.; Schmidt, C.; Morisette, J.; Morton, D. Validation of GOES and MODIS active fire detection products using ASTER and ETM+ data. *Remote Sens. Environ.* **2008**, *112*, 2711–2726. [CrossRef]
16. Giglio, L.; Schroeder, W.; Justice, C.O. The collection 6 MODIS active fire detection algorithm and fire products. *Remote Sens. Environ.* **2016**, *178*, 31–41. [CrossRef]
17. Filipponi, F. Exploitation of Sentinel-2 Time Series to Map Burned Areas at the National Level: A Case Study on the 2017 Italy Wildfires. *Remote Sens.* **2019**, *11*, 622. [CrossRef]
18. Van Leeuwen, W.J.; Casady, G.M.; Neary, D.G.; Bautista, S.; Alloza, J.A.; Carmel, Y.; Wittenberg, L.; Malkinson, D.; Orr, B.J. Monitoring post-wildfire vegetation response with remotely sensed time-series data in Spain, USA and Israel. *Int. J. Wildland Fire* **2010**, *19*, 75–93. [CrossRef]
19. Chu, T.; Guo, X. Remote Sensing Techniques in Monitoring Post-Fire Effects and Patterns of Forest Recovery in Boreal Forest Regions: A Review. *Remote Sens.* **2014**, *6*, 470–520. [CrossRef]
20. Storey, E.A.; Stow, D.A.; O'Leary, J.F. Assessing postfire recovery of chamise chaparral using multi-temporal spectral vegetation index trajectories derived from Landsat imagery. *Remote Sens. Environ.* **2016**, *183*, 53–64. [CrossRef]
21. Filipponi, F.; Manfron, G. Observing Post-Fire Vegetation Regeneration Dynamics Exploiting High-Resolution Sentinel-2 Data. *Proceedings* **2019**, *18*, 10. [CrossRef]
22. Ichoku, C.; Ellison, L. Global top-down smoke-aerosol emissions estimation using satellite fire radiative power measurements. *Atmos. Chem. Phys. Discuss.* **2014**, *14*, 6643–6667. [CrossRef]
23. Patra, P.K.; Ishizawa, M.; Maksyutov, S.; Nakazawa, T.; Inoue, G. Role of biomass burning and climate anomalies for land-atmosphere carbon fluxes based on inverse modeling of atmospheric CO_2. *Glob. Biogeochem. Cycles.* **2005**, *19*, GB3005. [CrossRef]
24. Boschetti, L.; Roy, D.P. Defining a fire year for reporting and analysis of global interannual fire variability. *J. Geophys. Res.* **2008**, *113*, G03020. [CrossRef]
25. Casa, R.; Castaldi, F.; Pascussi, S.; Pignatti, S. Chlorophyll estimation in field crops: An assessment of handheld leaf meters and spectral reflectance measurements. *J. Agric. Sci.* **2015**, *153*, 876–890. [CrossRef]
26. Xie, Q.; Dash, J.; Huang, W.; Peng, D.; Qin, Q.; Mortimer, H.; Casa, R.; Pignatti, S.; Laneve, G.; Pascucci, S.; et al. Vegetation indices combining the Red and Red-Edge spectral information for Leaf Area Index retrieval. *IEEE J. Sel. Top. Appl. Earth Obs. Remote Sens.* **2018**, *11*, 1482–1493. [CrossRef]
27. Filipponi, F. BAIS2: Burned Area Index for Sentinel-2. Multidisciplinary Digital Publishing Institute. *Proceedings* **2018**, *2*, 364. [CrossRef]
28. Axel, A.C. Burned Area Mapping of an Escaped Fire into Tropical Dry Forest in Western Madagascar Using Multi-Season Landsat OLI Data. *Remote Sens.* **2018**, *10*, 371. [CrossRef]
29. Pereira, J.M.C. A comparative evaluation of NOAA/AVHRR vegetation indexes for burned surface detection and mapping. *IEEE Trans. Geosci. Remote Sens.* **1999**, *37*, 217–226. [CrossRef]
30. Roy, D.P.; Boschetti, L.; Trigg, S.N. Remote sensing of fire severity: Assessing the performance of the normalized burn ratio. *IEEE Geosci. Remote Sens. Lett.* **2005**, *3*, 112–116. [CrossRef]
31. Bastarrika, A.; Chuvieco, E.; Pilar Martín, M. Mapping burned areas from Landsat TM/ETM + data with a two-phase algorithm: Balancing omission and commission errors. *Remote Sens. Environ.* **2011**, *115*, 1003–1012. [CrossRef]

32. Veraverbeke, S.; Lhermitte, S.; Verstraeten, W.W.; Goossens, R. Evaluation of pre/post-fire differenced spectral indices for assessing burn severity in a Mediterranean environment with Landsat Thematic Mapper. *Int. J. Remote Sens.* **2011**, *32*, 3521–3537. [CrossRef]
33. Lasaponara, R. Estimating spectral separability of satellite derived parameters for burned areas mapping in the Calabria region by using SPOT-Vegetation data. *Ecol. Model.* **2006**, *196*, 265–270. [CrossRef]
34. Stroppiana, D.; Boschetti, M.; Zaffaroni, P.; Brivio, P.A. Analysis and Interpretation of Spectral Indices for Soft Multicriteria Burned-Area Mapping in Mediterranean Regions. *IEEE Geosci. Remote Sens. Lett.* **2009**, *6*, 499–503. [CrossRef]
35. Stroppiana, D.; Bordogna, G.; Carrara, P.; Boschetti, M.; Boschetti, L.; Brivio, P.A. A method for extracting burned areas from Landsat TM/ETM+ images by soft aggregation of multiple Spectral Indices and a region growing algorithm. *ISPRS J. Photogramm. Remote Sens.* **2012**, *69*, 88–102. [CrossRef]
36. Kolden, C.A.; Lutz, J.A.; Key, C.H.; Kane, J.T.; van Wagtendonk, J.W. Mapped versus actual burned area within wildfire perimeters: Characterizing the unburned. *For. Ecol. Manag.* **2012**, *286*, 38–47. [CrossRef]
37. Lozano, F.J.; Suárez-Seoane, S.; de Luis, S. Assessment of several spectral indices derived from multi-temporal Landsat data for fire occurrence probability modeling. *Remote Sens. Environ.* **2007**, *107*, 533–544. [CrossRef]
38. Stroppiana, D.; Bordogna, G.; Boschetti, M.; Carrara, P.; Boschetti, L. Positive and Negative Information for Assessing and Revising Scores of Burn Evidence. *IEEE Geosci. Remote Sens. Lett.* **2012**, *9*, 363–367. [CrossRef]
39. Li, Z.; Kaufman, Y.J.; Ichoku, C.; Fraser, R.; Trishchenke, A.; Giglio, L.; Jin, J.; Yu, X. A review of AVHRR-based active fire detection algorithms: Principles, limitations, and recommendations. In *Global and Regional Vegetation Fire Monitoring From Space. Planning a Coordinated and International Effort*; Ahern, F.J., Goldammer, J.G., Justice, C.O., Eds.; SPB Academic: The Hague, The Netherlands, 2001; pp. 199–225.
40. Forman, R.T.T.; Godron, M. *Landscape Ecology*; J. Wiley and Sons: New York, NY, USA, 1986; p. 640.
41. Zonneveld, I.S. *Land Ecology: An Introduction to Landscape Ecology as a Base for Land Evaluation. Land Management and Conservation.*; SPB Academic Publishing: Amsterdam, The Netherlands, 1995; p. 199.
42. Bonan, G.B.; Levis, S.; Kergoat, L.; Oleson, K.W. Landscapes as patches of plant functional types: An integrating concept for climate and ecosystem model. *Global Biogeochem. Cycles* **2002**, *16*, 5. [CrossRef]
43. Poulter, B.; MacBean, N.; Hartley, A.; Khlystova, I.; Arino, O.; Betts, R.; Bontemps, S.; Boettcher, M.; Brockmann, C.; Defourny, P.; et al. Plant functional type classification for earth system models: Results from the European Space Agency's Land Cover Climate Change Initiative. *Geosci. Model Dev.* **2015**, *8*, 2315–2328. [CrossRef]
44. Fernández-Manso, A.; Fernández-Manso, O.; Quintano, C. SENTINEL-2A red-edge spectral indices suitability for discriminating burn severity. *Int. J. Appl. Earth Obs. Geoinf.* **2016**, *50*, 170–175. [CrossRef]
45. Huang, H.; Roy, D.P.; Boschetti, L.; Zhang, H.K.; Yan, L.; Kumar, S.S.; Gomez-Dans, J.; Li, J. Separability analysis of Sentinel-2A multi-spectral instrument (MSI) data for burned area discrimination. *Remote Sens.* **2016**, *8*, 873. [CrossRef]
46. Navarro, G.; Caballero, I.; Silva, G.; Parra, P.C.; Vázquez, A.; Caldeira, R. Evaluation of forest fire on Madeira Island using Sentinel-2A MSI imagery. *Int. J. Appl. Earth Obs. Geoinf.* **2017**, *58*, 97–106. [CrossRef]
47. Fernández-Manso, A.; Quintano, C.A. Synergetic Approach to Burned Area Mapping Using Maximum Entropy Modeling Trained with Hyperspectral Data and VIIRS Hotspots. *Remote Sens.* **2020**, *12*, 858. [CrossRef]
48. Brivio, A.P.; Petrucci, B.; Boschetti, M.; Carrara, P.; Pepe, M.; Rampini, A.; Stroppiana, D.; Zaffaroni, P. A multi-year geographic database off ire affected areas derived from satellite images in the National parks of Italy. *Riv. Ital. Di Telerilevamento-Ital. J. Remote Sens.* **2009**, *41*, 65–78.
49. Pulvirenti, L.; Squicciarino, G.; Fiori, E.; Fiorucci, P.; Ferraris, L.; Negro, D.; Gollini, A.; Severino, M.; Puca, S. An Automatic Processing Chain for Near Real-Time Mapping of Burned Forest Areas Using Sentinel-2 Data. *Remote Sens.* **2020**, *12*, 674. [CrossRef]
50. Azar, R.; Stroppiana, D.; Bresciani, M.; Giardino, C.; Boschetti, M.; Brivio, P.A. Accuracy of fuzzy burned area mapping as a function of the aerosol parameterization of atmospheric correction. In Proceedings of the Remote Sensing for Agriculture, Ecosystems, and Hydrology, Dresden, Germany, 23–26 September 2013; SPIE-International Society for Optics and Photonics: Washington, DC, USA, 2013; Volume XV(8887), p. 88870M. [CrossRef]

51. Stroppiana, D.; Azar, R.; Calò, F.; Pepe, A.; Imperatore, P.; Boschetti, M.; Silva, J.M.N.; Lanari, R. Integration of Optical and SAR Data for Burned Area Mapping in Mediterranean Regions. *Remote Sens.* **2015**, *7*, 1320–1345. [CrossRef]
52. Pesaresi, S.; Galdenzi, D.; Biondi, E.; Casavecchia, S. Bioclimate of Italy: Application of the worldwide bioclimatic classification system. *J. Maps* **2014**, *10*, 538–553. [CrossRef]
53. Smiraglia, D.; Capotorti, G.; Guida, D.; Mollo, B.; Siervo, V.; Blasi, C. Land units map of Italy. *J. Maps* **2013**, *9*, 239–244. [CrossRef]
54. Hagolle, O.; Huc, M.; Desjardins, C.; Auer, S.; Richter, R. MAJA Algorithm Theoretical Basis Document. Available online: https://doi.org/10.5281/zenodo.1209633 (accessed on 7 December 2017).
55. Rouquié, B.; Hagolle, O.; Bréon, F.M.; Boucher, O.; Desjardins, C.; Rémy, S. Using Copernicus atmosphere monitoring service products to constrain the aerosol type in the atmospheric correction processor MAJA. *Remote Sens.* **2017**, *9*, 1230. [CrossRef]
56. Csiszar, I.; Loboda, T.; French, N.H.F.; Giglio, L.; Hockenberry, T.L. *A multisensory Approach to Fine-Scale Characterization*; University of Maryland: College Park, MD, USA, 2014; p. 4.
57. Chuvieco, E.; Martin, M.P.; Palacios, A. Assessment of different spectral indices in the red-near-infrared spectral domain for burned land discrimination. *Int. J. Remote Sens.* **2002**, *23*, 5103–5110. [CrossRef]
58. Hislop, S.; Jones, S.; Soto-Berelov, M.; Skidmore, A.; Haywood, A.; Nguyen, T.H. Using Landsat Spectral Indices in Time-Series to Assess Wildfire Disturbance and Recovery. *Remote Sens.* **2018**, *10*, 460. [CrossRef]
59. Trigg, S.; Flasse, S. An evaluation of different bi-spectral spaces for discriminating burned shrub savanna. *Int. J. Remote Sens.* **2001**, *22*, 2641–2647. [CrossRef]
60. Rouse, J., Jr.; Haas, R.H.; Schell, J.A.; Deering, D.W. Monitoring vegetation systems in the Great Plains with ERTS. *NASA Spec. Publ.* **1974**, *351*, 309.
61. Singh, A. Digital change detection techniques using remotely sensing data. *Int. J. Remote Sens.* **1989**, *10*, 989–1003. [CrossRef]
62. Kaufman, Y.J.; Remer, L.A. Detection of forests using mid-IR reflectance: An application for aerosol studies. *IEEE Trans. Geosci. Remote Sens.* **1994**, *32*, 672–683. [CrossRef]
63. Smith, A.M.S.; Drake, N.A.; Wooster, M.J.; Hudak, A.T.; Holden, Z.A.; Gibbons, C.J. Production of Landsat ETM+ reference imagery of burned areas within Southern African savannahs: Comparison of methods and application to MODIS. *Int. J. Remote Sens.* **2007**, *28*, 2753–2775. [CrossRef]
64. Zanetti, M.; Marinelli, D.; Bertoluzza, M.; Saha, S.; Bovolo, F.; Bruzzone, L.; Magliozzi, M.L.; Zavagli, M.; Costantini, M. A high resolution burned area detector for Sentinel-2 and Landsat-8. In Proceedings of the 10th International Workshop on the Analysis of Multitemporal Remote Sensing Images (MultiTemp 2019), Shanghai, China, 5–7 August 2019.
65. Bovio, G. Method for forest fire damage level assessment based on detectable effects. In *Evaluation of Forest Fire Damages in Italy*; Ciancio, O., Corona, P., Marinelli, M., Pettenella, D., Eds.; Accademia Italiana di Scienze Forestali: Florence, Italy, 2007; pp. 55–60.